

Unstable Modes and Confinement in the Lattice Schrödinger Functional Approach

Paolo Cea^{a,b,1} and Leonardo Cosmai^{a,2}

^a*INFN - Sezione di Bari - Via Amendola, 173 - I 70126 Bari - Italy*

^b*Dipartimento di Fisica Univ. Bari - Via Amendola, 173 - I 70126 Bari - Italy*

Abstract

We analyze the problem of the Nielsen-Olesen unstable modes in the SU(2) lattice gauge theory by means of a recently introduced gauge-invariant effective action. We perform numerical simulations in the case of a constant Abelian chromomagnetic field. We find that for lattice sizes above a certain critical length the density of effective action shows a behaviour compatible with the presence of the unstable modes. We put out a possible relation between the dynamics of the unstable modes and the confinement.

1 Introduction

It is well known since long time that for non-Abelian gauge theories without matter fields in the one-loop approximation states with an external constant Abelian chromomagnetic field lies below the perturbative ground states. In the case of the SU(2) gauge theory the vacuum energy density turns out to be [1] in the one-loop approximation

$$\varepsilon(H) = \frac{1}{2}H^2 + \frac{11}{48\pi^2}g^2H^2 \ln\left(\frac{gH}{\Lambda^2}\right) + \mathcal{O}(g^2H^2), \quad (1)$$

where H is the strength of the external magnetic field. The energy density Eq.(1) has a negative minimum at some non zero value of the external field H . However, N. K. Nielsen and P. Olesen [2] pointed out that the Savvidy

¹ E-mail: cea@bari.infn.it

² E-mail: cosmai@bari.infn.it

states are not stable due to long-range modes: the Nielsen-Olesen unstable modes.

In a series of papers the proposal was advanced that the stabilization of the Nielsen-Olesen unstable modes results in the formation of a quantum liquid, the so-called Copenhagen vacuum [3].

The problem of the Nielsen-Olesen unstable modes has been reconsidered by using variational techniques on a class of gauge-invariant Gaussian wave functionals [4,5]. It turned out that the unstable modes contribute to the vacuum energy density with a negative classical term. In particular, in Ref. [5] it was shown that the Nielsen-Olesen modes get stabilized by considering configurations which differ from the classical external field only in the unstable sector. Moreover, the configurations which minimize the energy density screen almost completely the classical external chromomagnetic field and contribute to the energy density with a negative classical term that cancels the positive classical term in Eq.(1). However, it was pointed out that the calculation of the one-loop contribution to the vacuum energy density is truly non-perturbative and needs a completely non-perturbative approach.

Several authors studied gauge theories with an external background field on the lattice, both in three [6,7] and four [8,9] space-time dimensions. In particular, the results of Refs. [6] and [9] showed some evidence indicating the presence of the unstable modes. In those papers, however, the external background field was introduced via an external source. As a consequence the lattice effective action loses the manifest gauge invariance, for the source term in the lattice action becomes invariant only under a subgroup of the gauge group.

The aim of the present paper is to analyze the problem of the unstable modes in the case of the SU(2) lattice gauge theory by means of the recently introduced gauge invariant effective action [10].

2 SU(2) in a Constant Background Field

Let us consider a static external background field $\vec{A}_a^{\text{ext}}(\vec{x})$. We define the effective action which is invariant against gauge transformation of the external field by using the so-called Schrödinger functional:

$$\mathcal{Z} [\vec{A}_a^{\text{ext}}] = \langle \vec{A}_a^{\text{ext}} | \exp(-HT) \mathcal{P} | \vec{A}_a^{\text{ext}} \rangle, \quad (2)$$

where \mathcal{P} projects onto the physical states. On the lattice we can rewrite $\mathcal{Z}[\vec{A}_a^{\text{ext}}]$ as follows

$$\mathcal{Z}[\vec{A}_a^{\text{ext}}] = \int \mathcal{D}U \exp(-S_W), \quad (3)$$

where S_W is the standard Wilson action, and we integrate over the lattice links $U_\mu(x)$ with the constraints

$$U_\mu(x)|_{x_4=0} = U_\mu^{\text{ext}}(\vec{x}, 0). \quad (4)$$

The external links are related to the continuum gauge field \vec{A}_a^{ext} by the well-known relation

$$U_\mu^{\text{ext}}(x) = \text{P exp} \left\{ +iag \int_0^1 dt A_\mu^{\text{ext}}(x + at\hat{\mu}) \right\} \quad (5)$$

with $A_0^{\text{ext}}(\vec{x}) = 0$ and $\vec{A}^{\text{ext}}(\vec{x}) = \vec{A}_a^{\text{ext}}(\vec{x})\lambda_a/2$, and P is the path-ordering operator. It should be emphasized that the lattice Schrödinger functional has a well-defined continuum limit and, due to the gauge-invariance, does not require extra counterterms [11]. The lattice effective action for the external background field $\vec{A}_a^{\text{ext}}(\vec{x})$ is given by

$$\Gamma[\vec{A}^{\text{ext}}] = -\frac{1}{T} \ln \left\{ \frac{\mathcal{Z}[\vec{A}^{\text{ext}}]}{\mathcal{Z}(0)} \right\} \quad (6)$$

where T is the extension in the Euclidean time. It is straightforward to show that, in the limit $T \rightarrow \infty$, $\Gamma[\vec{A}^{\text{ext}}]$ reduces to the vacuum energy in presence of the given background field. Thus, our effective action is relevant to investigate non perturbatively the properties of the quantum vacuum.

In this paper we are interested in the case of a constant abelian chromomagnetic field for the SU(2) gauge theory

$$\vec{A}_a^{\text{ext}}(\vec{x}) = \vec{A}^{\text{ext}}(\vec{x})\delta_{a,3}, \quad A_k^{\text{ext}}(\vec{x}) = \delta_{k,2}x_1H. \quad (7)$$

Note that, due to the gauge invariance, $\Gamma[\vec{A}^{\text{ext}}]$ depends on the constant field strength $F_{12}^3 = H$. Thus, the relevant quantity is the density of the effective action:

$$\varepsilon[\vec{A}^{\text{ext}}] = -\frac{1}{\Omega} \ln \left[\frac{\mathcal{Z}[\vec{A}^{\text{ext}}]}{\mathcal{Z}(0)} \right], \quad (8)$$

where $\Omega = V \cdot T$, and V is the spatial volume. The external links corresponding to \vec{A}_a^{ext} are easily evaluated from Eq.(5). We get

$$\begin{aligned}
U_2^{\text{ext}}(\vec{x}, 0) &= \cos\left(\frac{agHx_1}{2}\right) + i\sigma^3 \sin\left(\frac{agHx_1}{2}\right) \\
U_1^{\text{ext}}(\vec{x}, 0) &= U_3^{\text{ext}}(x) = U_4^{\text{ext}}(x) = 1.
\end{aligned} \tag{9}$$

By imposing the periodic boundary conditions we obtain the quantization condition

$$\frac{a^2 g H}{2} = \frac{2\pi}{L_1} n^{\text{ext}} \tag{10}$$

where n^{ext} is an integer, L_1 the lattice extension in the x_1 direction (in lattice units).

3 The Unstable Modes

Let us now briefly discuss the origin of the unstable modes both in the continuum and on the lattice.

In order to evaluate the one-loop effective action in the continuum one writes

$$A_\mu^a(x) = \bar{A}_\mu^a(x) + \eta_\mu^a(x) \tag{11}$$

where $\bar{A}_\mu^a(x) = \delta_{\mu 2} \delta^{a3} x_1 H$ and $\eta(x)$ is the quantum fluctuation on the background field. In the background gauge

$$(\delta^{ab} \partial_\mu - g \varepsilon^{abc} \bar{A}_\mu^c) \eta_\mu^b(x) = 0, \tag{12}$$

we rewrite the pure gauge action in the one-loop approximation as

$$S_{Y-M} = S_{\text{class}} + \frac{1}{2} \int d^4x \eta_\mu^a(x) \mathcal{O}_{\mu\nu}^{ab} \eta_\nu^b(x). \tag{13}$$

The one-loop effective action can be obtained by performing the Gaussian functional integrations over the quantum fluctuations and including the Faddeev-Popov one-loop determinant. However, if we solve the eigenvalue equations

$$\mathcal{O}_{\mu\nu}^{ab} \phi_\nu^b(x) = \lambda \phi_\mu^a(x), \tag{14}$$

then we find that there are negative eigenvalues:

$$\lambda_u = p_0^2 + p_3^2 - gH. \tag{15}$$

Indeed $\lambda_u < 0$ when $gH > p_0^2 + p_3^2$. The modes with eigenvalue λ_u are the Nielsen-Olesen unstable modes. If we perform formally the Gaussian functional integration, then the one-loop effective action picks out an imaginary part. The point is that in the functional integration over the unstable modes

one must include the positive quartic term. If we do that, we find that the unstable modes behave like a two-dimensional tachyonic charged scalar field. Thus the stabilization of the unstable modes resemble the (dynamical) Higgs mechanism. The negative condensation energy we gain in the stabilization procedure cancels the positive classical magnetic energy [5].

On the lattice we would like to evaluate the Schrödinger functional Eq.(3) in the weak coupling region. To this end, we write [11] the lattice version of Eq.(11):

$$U_\mu(x) = \exp(iagq_\mu(x)) U_\mu^{\text{ext}}(x), \quad (16)$$

where the fluctuations $q_\mu(x) = q_\mu^a(x)\sigma^a/2$ satisfy the boundary conditions

$$q_\mu(x)|_{x_4=0} = 0. \quad (17)$$

Inserting Eq.(16) into the Wilson action we obtain in the one-loop approximation

$$S_W = S^{\text{ext}} + S^{(2)} \quad (18)$$

where

$$S^{\text{ext}} = \frac{4\Omega}{g^2} \left[1 - \cos\left(\frac{gH}{2}\right) \right] \quad (19)$$

and $S^{(2)}$ is quadratic in the quantum fluctuations $q_\mu(x)$. We are interested in the spectrum of the lattice version of the operator $\mathcal{O}_{\mu\nu}^{ab}$ in Eq.(14). Unfortunately the discrete eigenvalue equation cannot be solved (analytically) in closed form. Obviously it is possible to solve the eigenvalue equation by means of numerical methods. We plan to discuss this matter in a future paper. Nevertheless, if we discard a lot of irrelevant operators in $S^{(2)}$, i.e. terms which vanish in the naive continuum limit, we find an approximate formula for the eigenvalues. In particular the unstable mode eigenvalue turns out to be

$$\lambda_u = (1 - \cos p_4) + (1 - \cos p_3) - \sin\left(\frac{gH}{2}\right). \quad (20)$$

By using Eq.(10) and $p_\mu = 2\pi n_\mu/L_\mu$, we get

$$\lambda_u = 1 - \cos\left(\frac{2\pi}{L_4}n_4\right) + 1 - \cos\left(\frac{2\pi}{L_3}n_3\right) - \sin\left(\frac{2\pi}{L_1}n^{\text{ext}}\right). \quad (21)$$

4 Monte Carlo Simulations

We performed our Monte Carlo simulations on lattices with linear sizes $L_1 = L_4 = 32$, $L_2 = L_3 = L$ and $n^{\text{ext}} = 1$. Inserting these values into Eq.(21), it fol-

lows that $\lambda_u < 0$ when $L \geq L_{\text{crit}}$, $L_{\text{crit}} \simeq 10$. Remarkably, these considerations suggest that we can switch on and off the unstable modes by varying L .

We turn now on discussing the outcomes of the numerical simulations. We are interested in the vacuum energy density Eq.(8). To avoid the problem of computing a partition function, we focus on the derivative of $\varepsilon[\vec{A}^{\text{ext}}]$ with respect to β by taking n^{ext} (i.e. gH , see Eq.(10)) fixed. A straightforward calculation gives:

$$\varepsilon'[\vec{A}^{\text{ext}}] = \left\langle \frac{1}{\Omega} \sum_{x, \mu > \nu} \frac{1}{2} \text{Tr} U_{\mu\nu}(x) \right\rangle_0 - \left\langle \frac{1}{\Omega} \sum_{x, \mu > \nu} \frac{1}{2} \text{Tr} U_{\mu\nu}(x) \right\rangle_{A^{\text{ext}}} \quad (22)$$

where the $U_{\mu\nu}(x)$'s are the plaquettes in the (μ, ν) plane. As we said, our simulations are performed on $32 \times L^2 \times 32$ lattices with $L = 6, 8, 10, 16, 20, 24$. We impose periodic boundary conditions. We use standard overrelaxed Metropolis algorithm to update gauge configurations. The links belonging to the time slice $x_4 = 0$ are frozen according to Eq.(9). Moreover, we also impose that the links at the spatial boundaries are fixed according to Eq.(9). Note that this condition corresponds in the continuum to the usual requirement that the fluctuations over the background field vanish at the spatial infinity. It is obvious that the contributions to $\varepsilon'[\vec{A}^{\text{ext}}]$ due to the frozen time slice at $x_4 = 0$ and to the fixed links at the lattice spatial boundaries must be subtracted, i.e. only the dynamical links must be taken into account in evaluating $\varepsilon'[\vec{A}^{\text{ext}}]$. We denote by $\Omega = L_1 L_2 L_3 L_4$ the total number of lattice sites (i.e. the lattice volume) belonging to the lattice Λ . Ω_{ext} are the lattice sites whose links are fixed according to Eq.(9):

$$\Omega_{\text{ext}} = L_1 L_2 L_3 + (L_4 - 1) \times (L_1 L_2 L_3 - (L_1 - 2)(L_2 - 2)(L_3 - 2)). \quad (23)$$

Hence $\Omega_{\text{int}} = \Omega - \Omega_{\text{ext}}$ is the volume occupied by the “internal” lattice sites (let us denote this ensemble by $\tilde{\Lambda}$). Accordingly we define the derivative of the “internal” energy density $\varepsilon'_{\text{int}}$ as

$$\varepsilon'_{\text{int}}[\vec{A}^{\text{ext}}] = \left\langle \frac{1}{\Omega_{\text{int}}} \sum_{x \in \tilde{\Lambda}, \mu > \nu} \frac{1}{2} \text{Tr} U_{\mu\nu}(x) \right\rangle_0 - \left\langle \frac{1}{\Omega_{\text{int}}} \sum_{x \in \tilde{\Lambda}, \mu > \nu} \frac{1}{2} \text{Tr} U_{\mu\nu}(x) \right\rangle_{A^{\text{ext}}}. \quad (24)$$

In Figures 1 and 2 we report the derivative of the internal energy density versus β in units of the derivative of the energy density due to the “external” links defined in Eq.(9)

$$\varepsilon'_{\text{ext}} = \frac{\partial}{\partial \beta} \frac{1}{\Omega} S^{\text{ext}} = 1 - \cos\left(\frac{2\pi}{L_1} n^{\text{ext}}\right). \quad (25)$$

Several features of Fig. 1 are worth noting. In the strong coupling region $\beta \lesssim 1$ the external background field is completely shielded. This behavior is

very similar to the one we found for the U(1) gauge theory [10]. Moreover, $\varepsilon'_{\text{int}}$ displays a peak at $\beta \simeq 2.2$. These features are displayed also [12] by the specific heat in pure SU(2). This is not surprising, for our previous studies [10,13] in U(1) showed that $\varepsilon'_{\text{int}}$ behaves as the specific heat.

The derivative of the internal energy density displays the most interesting behavior in the weak coupling region $\beta \gtrsim 2.3$. Indeed, we feel that this peculiar behavior is due to the unstable modes. To see this, we recall that according to our previous discussion we have in the weak coupling region

$$\varepsilon_{\text{int}}(\beta, n^{\text{ext}}) = \beta \left[1 - \cos \left(\frac{2\pi}{L_1} n^{\text{ext}} \right) \right] + g(n^{\text{ext}}) + \mathcal{O} \left(\frac{1}{\beta} \right). \quad (26)$$

The first term in Eq.(26) is the classical magnetic energy, while $g(n^{\text{ext}})$ is the one-loop contribution. As a consequence we expect that

$$\varepsilon'_{\text{int}}(\beta, n^{\text{ext}}) = 1 - \cos \left(\frac{2\pi}{L_1} n^{\text{ext}} \right) + \mathcal{O} \left(\frac{1}{\beta^2} \right). \quad (27)$$

Equation (27) tells us that, in the weak coupling region the derivative of the vacuum energy density reduces to $\varepsilon'_{\text{ext}}$. Indeed, in the U(1) gauge theory this is the case [10]. From Figure 1 we see that, for $L \simeq 6 - 8$, $\varepsilon'_{\text{int}}$ tends to $\varepsilon'_{\text{ext}}$ (in the weak coupling region) as in U(1). However, by increasing L the ratio $\varepsilon'_{\text{int}}/\varepsilon'_{\text{ext}}$ decreases (see Fig. 2).

In order to ascertain if the effects displayed by our data are not due to the lattice artifacts, we contrast in Fig.3 the derivative of the vacuum energy density in the weak coupling region both for SU(2) and U(1) versus the lattice linear size L . As we can see, the ratio $\varepsilon'_{\text{int}}/\varepsilon'_{\text{ext}} \simeq 1$ and it is almost independent on L in the case of the U(1) theory. On the other hand, for the SU(2) case Fig.3 clearly shows that the ratio $\varepsilon'_{\text{int}}/\varepsilon'_{\text{ext}} \rightarrow 0$ in the infinite volume limit. As we shall argue in a moment, this peculiar behaviour can be ascribed to the unstable modes. To see this we recall that the stabilization of the unstable modes should modify Eq.(26) as follows [5]:

$$\varepsilon_{\text{int}}(\beta, n^{\text{ext}}) = g(n^{\text{ext}}) + \mathcal{O} \left(\frac{1}{\beta} \right). \quad (28)$$

However, in Ref. [5] it was pointed out that the cancellation of the classical energy term happens only in the thermodynamical limit $V \rightarrow \infty$. So that we expect that Eq.(28) holds on the infinite lattice. On a finite lattice we expect that in the weak coupling region

$$\frac{\varepsilon'_{\text{int}}}{\varepsilon'_{\text{ext}}} = f(x) + \mathcal{O} \left(\frac{1}{\beta^2} \right) \quad (29)$$

with $x = a_H/L_{\text{eff}}$, where $a_H = \sqrt{2\pi/gH}$ is the magnetic length and

$$L_{\text{eff}} = \Omega_{\text{int}}^{1/4}, \quad (30)$$

is the lattice effective linear size. The continuum calculations of Ref. [5] tell us that $f(0) = 0$. In Figure 4 we display the ratio $\varepsilon'_{\text{int}}/\varepsilon'_{\text{ext}}$ for $\beta = 5$ versus the lattice effective linear size. Indeed Fig.4 shows that $\varepsilon'_{\text{int}}$ decreases by increasing L_{eff} . So that we have $\varepsilon'_{\text{int}} \rightarrow 0$ when $L_{\text{eff}} \rightarrow \infty$, in agreement with Eq.(28). Moreover, we see clearly that a critical length exists such that for $L_{\text{eff}} \leq L_{\text{eff}}^{\text{crit}}$ Eq.(27) holds. It is remarkable that our estimation of the critical length

$$L_{\text{eff}}^{\text{crit}} \approx 12 \quad (31)$$

is in good agreement with Ref. [9]. Moreover, in the region $L_{\text{eff}} > L_{\text{eff}}^{\text{crit}}$ we fitted the data trying the power law

$$f(x) = kx^\alpha. \quad (32)$$

Indeed we find a rather good fit ($\chi^2/\text{d.o.f.} \simeq 0.3$, solid line in Fig.4) with

$$k = 5(1), \quad \alpha = 1.43(8). \quad (33)$$

In our opinion the existence of a critical length and the cancellation of the classical magnetic energy density in the thermodynamical limit constitute a rather strong evidence for the unstable modes on the lattice. Remarkably it turns out that also the peak value of $\varepsilon'_{\text{int}}$ tends towards zero with the same power law as implied by Eq. (33). Indeed, in Fig. 5 we show the ratio $\varepsilon'_{\text{int}}/\varepsilon'_{\text{ext}}$ taken at the peaks in Figs. 1 and 2. For $L_{\text{eff}} > L_{\text{eff}}^{\text{crit}}$ we find (solid line in Fig.5)

$$\frac{\varepsilon'_{\text{int}}}{\varepsilon'_{\text{ext}}} = k' \left(\frac{a_H}{L_{\text{eff}}} \right)^{\alpha'}, \quad (34)$$

where $k' = 10(2)$, $\alpha' = 1.5(1)$ and $\chi^2/\text{d.o.f.} \simeq 0.3$. Note that $\alpha' = \alpha$ within our statistical uncertainties. Thus Eqs. (29), (32), and (34) imply that $\varepsilon'_{\text{int}}[\vec{A}^{\text{ext}}]$ tends uniformly towards zero in the thermodynamical limit.

5 Conclusions

Let us conclude by stressing the main results of this paper.

By using the gauge invariant effective action for background fields on the lattice we studied non perturbatively the dynamics of the Nielsen-Olesen unstable modes. We feel that the existence of a critical length $L_{\text{eff}}^{\text{crit}}$ and the cancellation of the classical magnetic energy in the infinite volume limit constitute a strong

evidence for the unstable modes on the lattice. Moreover, our numerical results are suggesting that $\varepsilon' [\vec{A}^{\text{ext}}] \rightarrow 0$ when $L_{\text{eff}} \rightarrow \infty$ in the whole β -region. Thus in the continuum limit $L_{\text{eff}} \rightarrow \infty$, $\beta \rightarrow \infty$ the confining vacuum screens completely the external chromomagnetic Abelian field. In other words, the continuum vacuum behaves as an Abelian magnetic condensate medium in accordance with the dual superconductivity scenario. The magnetic condensate dynamics seems to be closely related to the presence of the Nielsen-Olesen unstable modes. In conclusion we feel that our approach to a gauge-invariant effective action on the lattice is a useful tool to understand the dynamics of color confinement.

References

- [1] G. K. Savvidy, Phys. Lett. **B71** (1977) 133; S. G. Matinyan and G. K. Savvidy, Nucl. Phys. **B134** (1978) 539; I. A. Balatin, S. G. Matinyan and G. K. Savvidy, Sov. J. Nucl. Phys. **26** (1978) 214.
- [2] N.K. Nielsen and P. Olesen, Nucl. Phys. **B144** (1978) 376.
- [3] For a review, see: H. B. Nielsen in *Particle Physics*, eds. I. Andrić, I. Dadić and N. Zovko (North-Holland, Amsterdam, 1981).
- [4] M. Consoli and G. Preparata, Phys. Lett. **154B** (1985) 411.
- [5] P. Cea, Phys. Rev. **D37** (1988) 1637.
- [6] P. Cea and L. Cosmai, Phys. Rev. **D48** (1993) 3364; P. Cea and L. Cosmai, hep-lat/9306007; P. Cea and L. Cosmai, Nucl. Phys. (Proc. Suppl.) **34** (1994) 234.
- [7] H. D. Trottier and R. M. Woloshyn, Phys. Rev. Lett. **70** (1993) 2053; E. **72** (1994) 4155.
- [8] J. Ambjorn, V. K. Mitriushkin, and A. M. Zadorozhny, Phys. Lett. **B245** (199) 575; P. Cea and L. Cosmai, Phys. Lett. **B264** (1991) 415.
- [9] A. R. Levi, Nucl. Phys. B (Proc. Suppl.) **34** (1994) 161; A. R. Levi and J. Polonyi, Phys. Lett. **B357** (1995) 186.
- [10] P. Cea, L. Cosmai, and A. D. Polosa, hep-lat/9601010.
- [11] M. Lüscher, R. Narayanan, P. Weisz, and U. Wolff, Nucl. Phys. **B384** (1992) 168; M. Lüscher and P. Weisz, Nucl. Phys. **B452** (1995) 213.
- [12] B. Lautrup and M. Nauenberg, Phys. Rev. Lett. **45** (1980) 1755; J. Engels and T. Scheideler, hep-lat/960741.
- [13] P. Cea, L. Cosmai, and A. D. Polosa, hep-lat/9607020.

FIGURE CAPTIONS

- Figure 1. $\varepsilon'_{\text{int}}[\vec{A}^{\text{ext}}]/\varepsilon'_{\text{ext}}$ versus β for $L = 6$ (stars) and $L = 8$ (crosses).
- Figure 2. $\varepsilon'_{\text{int}}[\vec{A}^{\text{ext}}]/\varepsilon'_{\text{ext}}$ versus β for $L = 10$ (diamonds), $L = 16$ (triangles) and $L = 24$ (circles).
- Figure 3. The ratio $\varepsilon'_{\text{int}}[\vec{A}^{\text{ext}}]/\varepsilon'_{\text{ext}}$ in the weak coupling region versus L for $U(1)$ (circles, $\beta = 3$) and $SU(2)$ (squares, $\beta = 5$).
- Figure 4. The ratio $\varepsilon'_{\text{int}}[\vec{A}^{\text{ext}}]/\varepsilon'_{\text{ext}}$ at $\beta = 5$ versus L_{eff} . The solid line is the fit Eq. (32).
- Figure 5. The ratio $\varepsilon'_{\text{int}}[\vec{A}^{\text{ext}}]/\varepsilon'_{\text{ext}}$ at the peak values versus L_{eff} . The solid line is the fit Eq. (34).

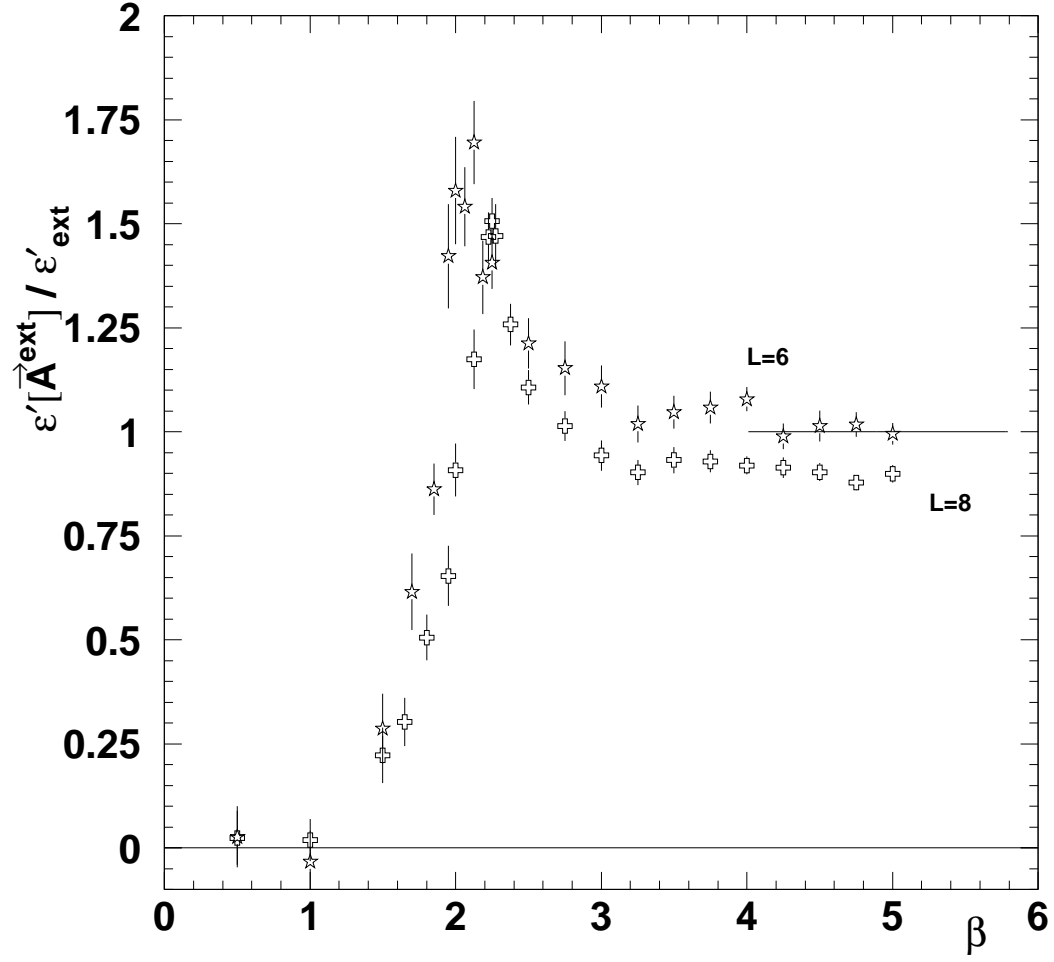


Fig. 1. $\varepsilon'_{\text{int}}[\vec{A}^{\text{ext}}] / \varepsilon'_{\text{ext}}$ versus β for $L = 6$ (stars) and $L = 8$ (crosses).

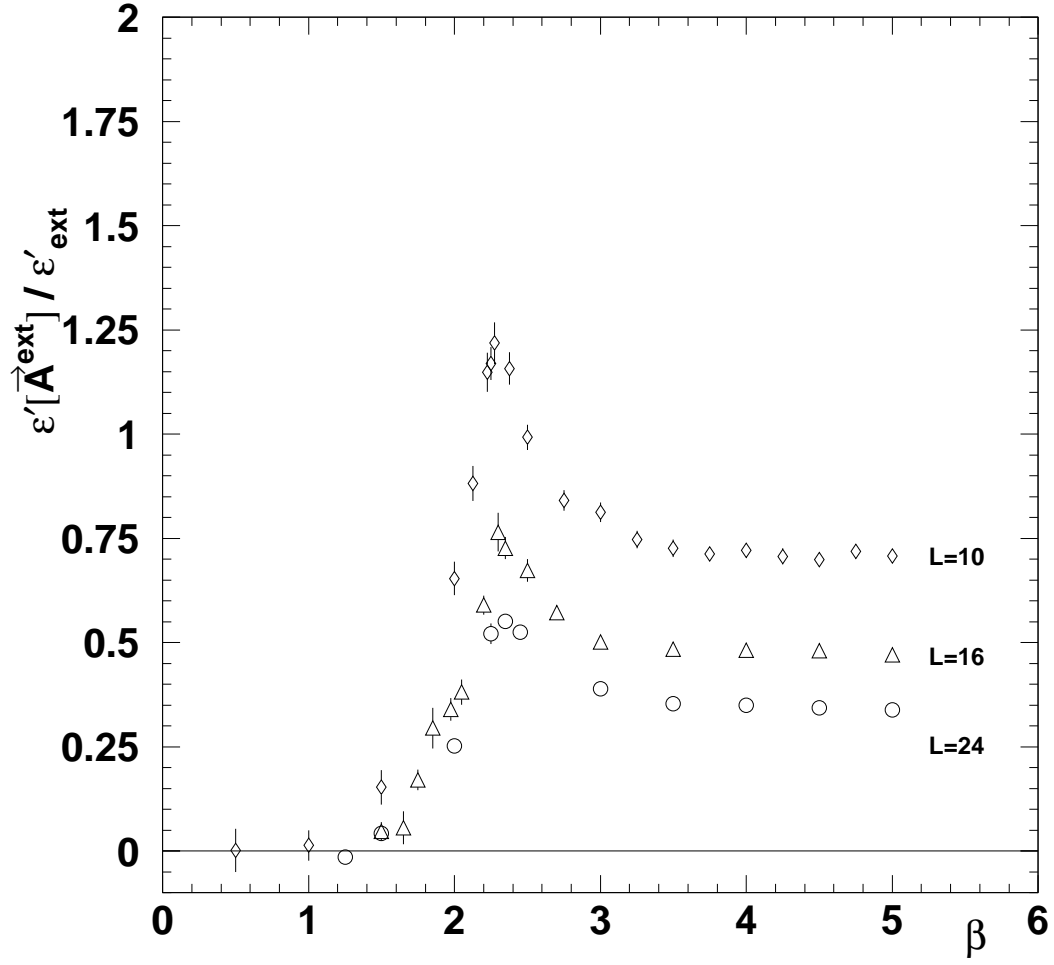


Fig. 2. $\varepsilon'_{\text{int}}[\vec{A}^{\text{ext}}]/\varepsilon'_{\text{ext}}$ versus β for $L = 10$ (diamonds), $L = 16$ (triangles) and $L = 24$ (circles).

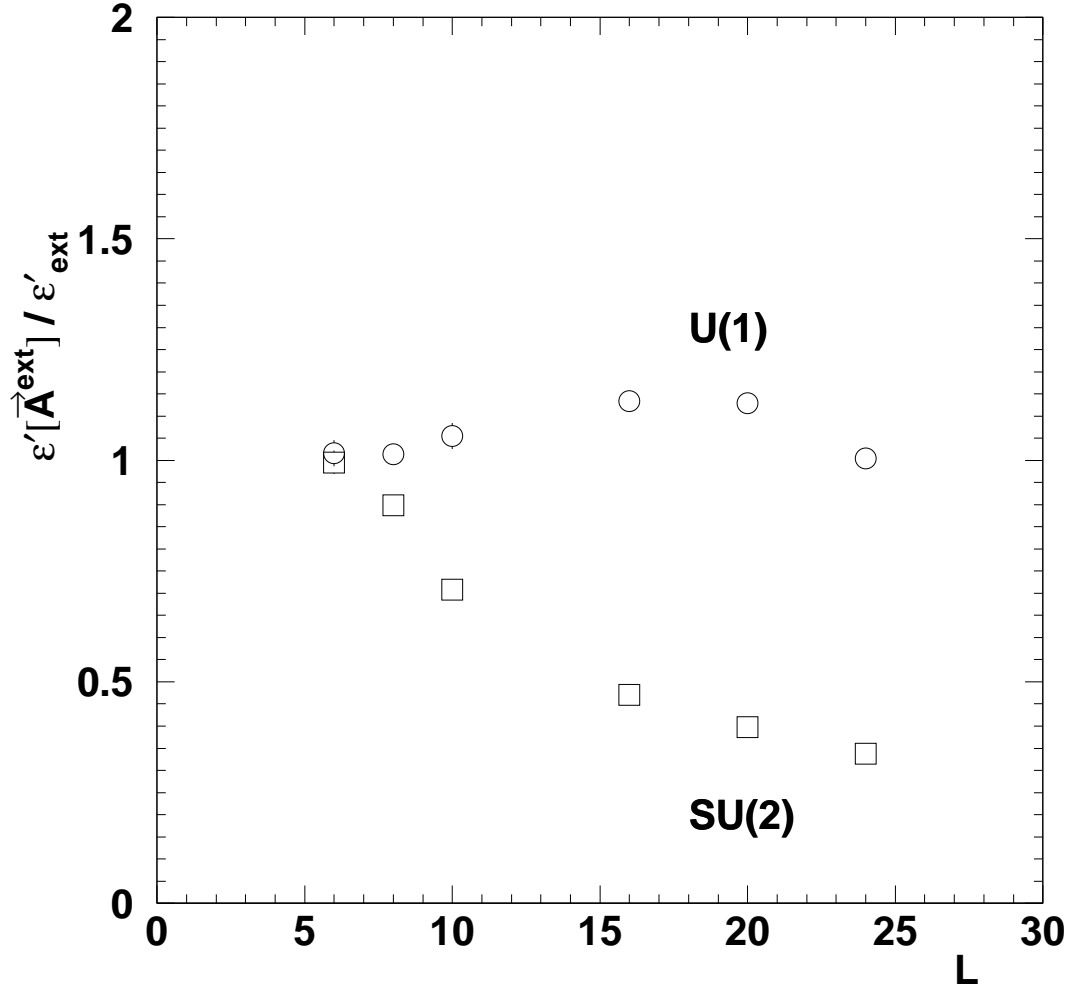


Fig. 3. The ratio $\varepsilon'_{\text{int}}[\vec{A}^{\text{ext}}]/\varepsilon'_{\text{ext}}$ in the weak coupling region versus L for $U(1)$ (circles, $\beta = 3$) and $SU(2)$ (squares, $\beta = 5$).

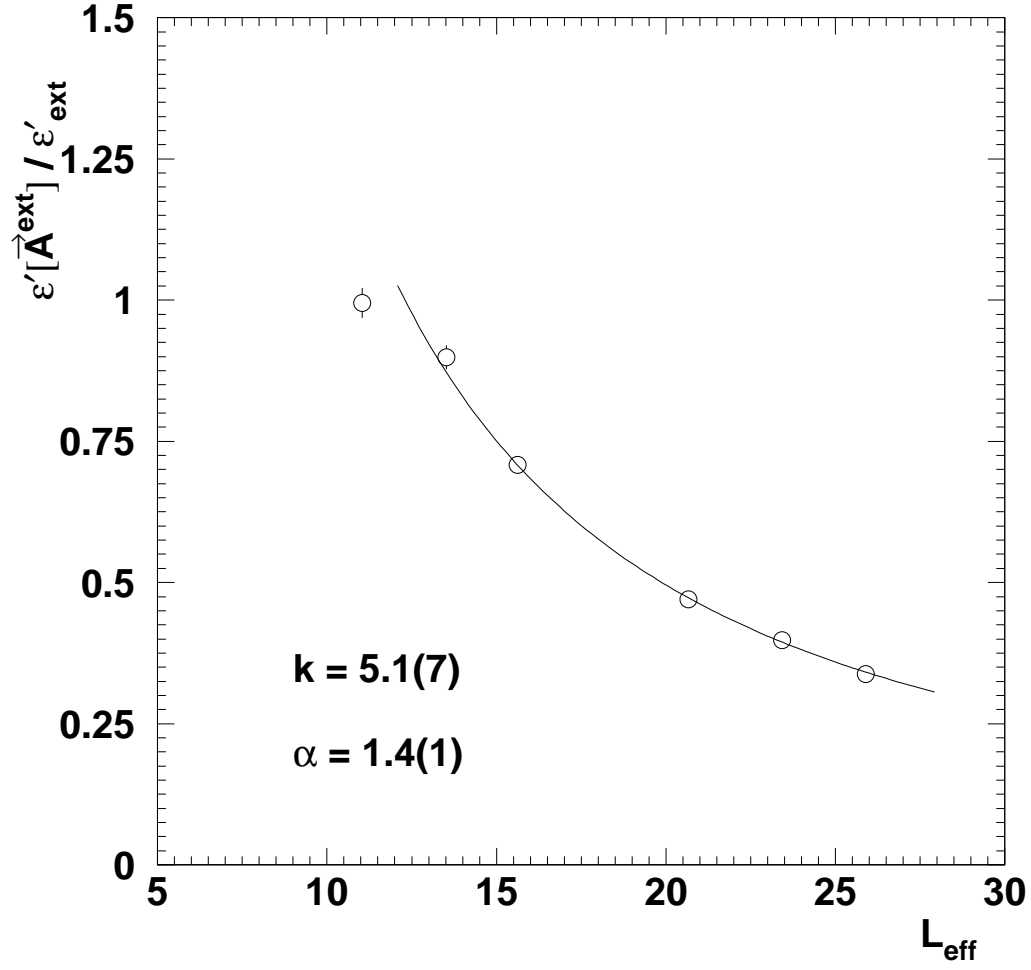


Fig. 4. The ratio $\varepsilon'_{\text{int}}[\vec{A}^{\text{ext}}]/\varepsilon'_{\text{ext}}$ at $\beta = 5$ versus L_{eff} . The solid line is the fit Eq. (32).

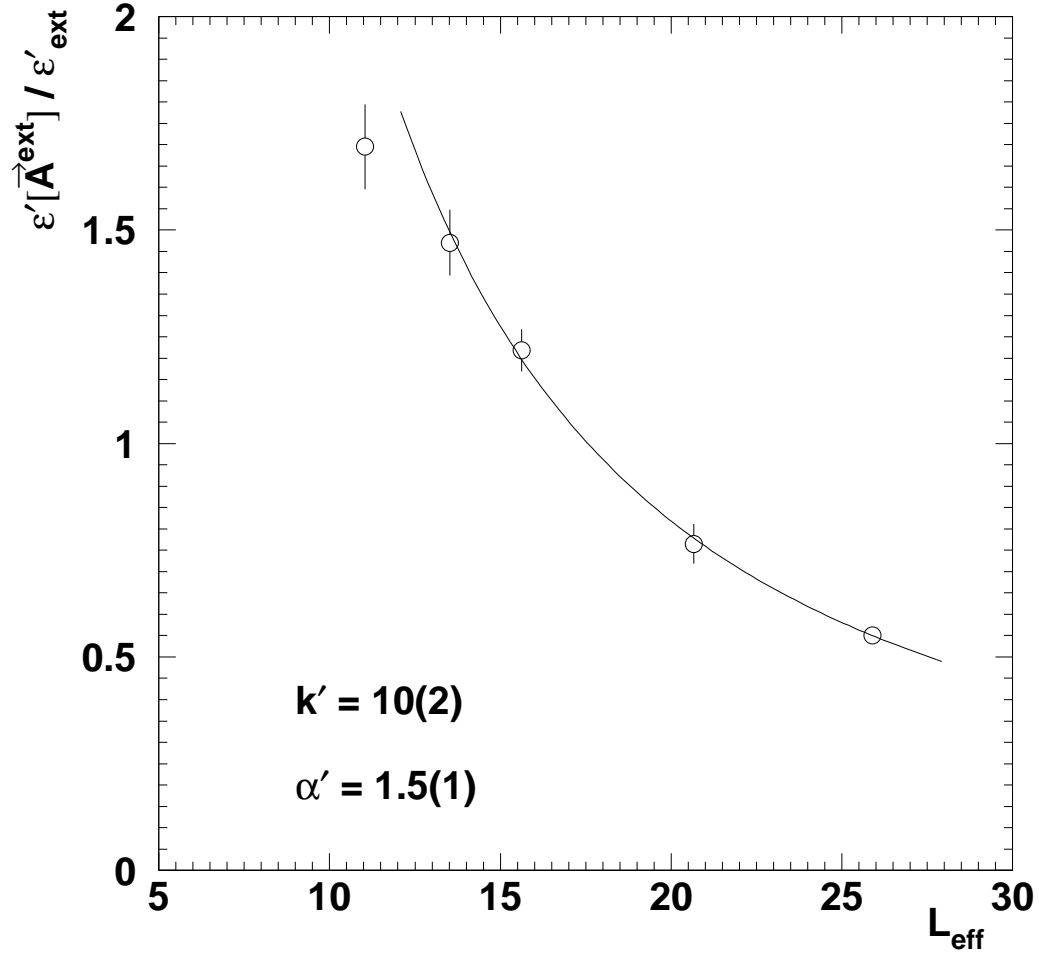


Fig. 5. The ratio $\varepsilon'_{\text{int}}[\vec{A}^{\text{ext}}]/\varepsilon'_{\text{ext}}$ at the peak values versus L_{eff} . The solid line is the fit Eq. (34).